JOURNAL OF MATERIALS SCIENCE **40** (2005) 3475 – 3480

Cell structure and compressive behavior of an aluminum foam

WANG DEQING*, XUE WEIWEI, MENG XIANGJUN, SHI ZIYUAN
College of Materials Science and Engineering, Dalian Jiaotong University, Dalian, Liaoning 116028, People's Republic of China
E-mail: wdeqing@online.ln.cn

The plastic collapse strength, energy absorption and elastic modulus of a closed cell aluminum foam are studied in relation to cell structures. The density, node size and the cell wall thickness of the aluminum foams decrease with increasing cell size. The failure of the foam cells under compressive load progresses successively from the top or/and bottom to the mid-layer of the compression specimens, and no initial rupture of the foam cells is observed in the mid-height of the foam samples. When foam density increases from 0.11 to 0.22 g/cm ^{3}, the plastic collapse strength rises from 0.20 to 1.29 MPa, while the elastic modulus of the closed cell aluminum foam increases from 0.70 to 1.17 GPa. In contrast, the energy absorption of the foams decreases rapidly with increasing cell size. When cell size increases from 4.7 to 10.1 mm, the energy absorption drops from over unity to 0.3 J/cm ^{3}. The normalized Yong's modulus of the closed cell aluminum foam is $E^*/E_s = 0.208\ (\rho^*/\rho_s)$, while the normalized strength of the foams, σ^*/σ_s is expressed by $\sigma^*/\sigma_s = c \cdot \rho^*/\rho_s$ where c is a density-dependent parameter. Furthermore, the plastic collapse strength and energy absorption ability of the closed cell aluminum foams are significantly improved by reducing cell size of the aluminum foams having the same density.

1. Introduction

Closed-cell aluminum foam offers a unique combination of properties such as low density, high stiffness and energy absorption [1–4]. Through design of microstructure, the properties of aluminum foams can be made to vary greatly for the demands of specific engineering applications. Closed-cell aluminum foams can be manufactured by introduction of air into molten aluminum composites [5–6]. The injected air causes bubbles to rise to the surface of the melt, forming a liquid foam which is stabilized by the presence of solid ceramic particles on the gas liquid interfaces of the cell walls. The stabilized liquid foams are then mechanically conveyed off the surface of the melt and allowed to cool to form a solid slab of aluminum foam. With the development of the technologies for the production of aluminum foams, researchers have long realized that the physical and mechanical properties of aluminum foams are not only governed by cell wall material and the volume fraction of the solid [3], but also affected significantly by the geometry of the cell structure [7, 8]. In the case of the closed-cell aluminum foam by air injection, the cell geometry (size and wall thickness) is controlled by the process variables including the shape and dimensions of foaming chamber, size and volume fraction of the solid particles, foaming temperature, air injection rate and impeller design and speed during foam production [9].

Although extensive studies have been carried out on compression properties of closed-cell aluminum foams [10–16], no reports have been found to relate the compression behavior of the foams to the effect of their cell structure parameters such as cell size and cell wall thickness. In order to control structure and property of the closed-cell aluminum foam, the current authors prepared the closed-cell aluminum foams with the same chemical composition but different cell sizes and structural parameters by changing foaming conditions. From an application perspective, the most important properties for closed cell aluminum foams are the elastic stiffness, the yield strength and the 'plateau' stress at which the foams compress plastically. Therefore, this paper reports mainly the relationships between compressive properties and cell structures of the closed-cell aluminum foams.

2. Experimental procedure

The specimens of the closed-cell aluminum foams were cut from the foam slabs which were prepared by injecting compressed air into an aluminum alloy melt with solid SiC particles as a foam stabilizer. The setup of

*Author to whom all correspondence should be addressed.

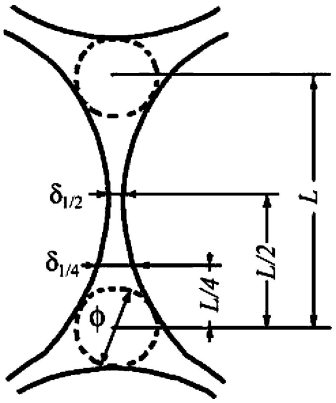

Figure 1 Schematic description of cell wall and node geometry.

the foaming experiments is shown in reference [9], and the detailed foaming procedures and the results will be published elsewhere.

The shape of the foam cells was observed visually on face and edge numbers. The macroscopic images of the foam structures were taken using an optical scanner, and the contrast of the foam surface was improved by spraying with black paint, and then the surface was ground to remove paint from the cell walls. The density of the aluminum foams, ρ^* was calculated by weight and dimensions of the specimens. Cell size, Φ was measured for at least 400 cells on six orthogonal surfaces of compression test specimens of the foams processed at different conditions by using mean intercept length technique. A sketch of the cell wall and node (Plateau border) geometry is shown in Fig. 1 where the cell wall thickness, $\delta_{1/2}$ and $\delta_{1/4}$ at *L/2* and *L/4* of the chord length L were measured using a digital caliper with 1 μm resolution, and the node size, ϕ was measured under microscope (avoiding distortion caused by the angle of sectioning). 20 mean-sized cells were selected for the measurement of wall thickness and node size of the closed cell aluminum foam, and average values were taken for their corresponding dimensions.

Yield strength of the cell walls, σ_s was measured by indentation and was taken to be one-third of the hardness value of the solid foam material [18]. The samples for microhardness test were cut from an ingot of a solidified foam melt, mounted in a cold setting resin and polished. Indentations were made by a computerized FM-700 Vickers micro-hardometer under a load of 25 g for 20 s. The microhardness was evaluated by taking ten indentations, and only the eight middle values were averaged.

Compression specimens with a cross-section of 90 × 90 mm^2 and height of 40–80 mm were cut from foam slabs with different foaming conditions. The height of the compression specimens was at least seven times of the cell size in order to avoid sample edge effect on measuring elastic modulus and plastic collapse strength [11]. Uniaxial compression tests were conducted under a servohydraulic testing machine. The stress curves were plotted against nominal strain, ε, (calculated on the basis of the initial specimen height and the crosshead displacement of compression test machine). The plastic collapse strength, σ^* (defined as the first peak stress before the onset of load drop due to plastic instability), and energy absorption per unit volume, W (defined as the area under the stress-strain curve obtained prior to the onset of densification), were measured. The onset of densification is arbitrarily determined by 50% of height reduction of the compression samples. The Young's modulus of the foam, E^* was calculated from the slope of the unloading load-deflection curve taken at approximately 75% of the plastic collapse stress of the foams.

3. Results and discussion

3.1. Cell structure

The representative morphologies of the aluminum foams are shown in Fig. 2. The closed cell foams of both the high and low densities have relatively uniform cell size and distribution, and no defects such as crack, void and cell wall corrugation are observed for the both large and small celled aluminum foams. The cell wall curvature, although existed, were not characterized due to the uniform distribution of cell sizes for all the foams. Macrostructurally, all the foams with large or small cell sizes prepared under the foaming conditions are characterized as low density foams consisting of roughly equiaxed polyhedral cells which differ from the more

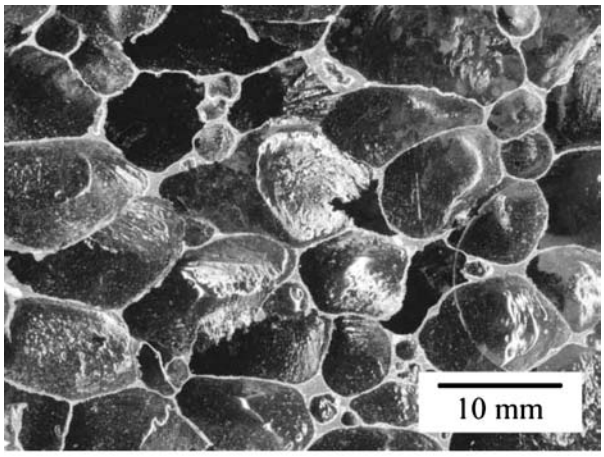

(a)

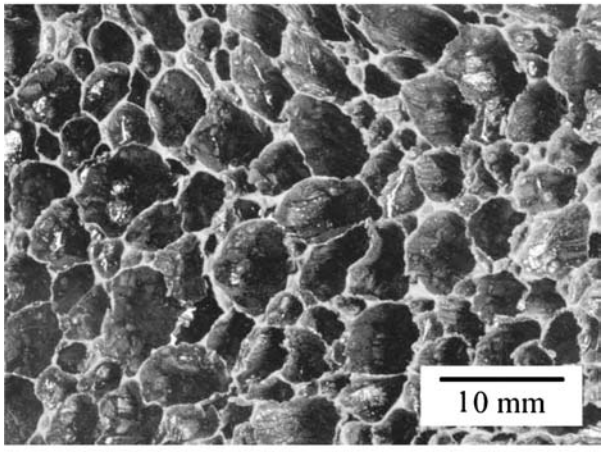

(b)

Figure 2 Macrograph of the aluminum foam with (a) large and (b) small cells.

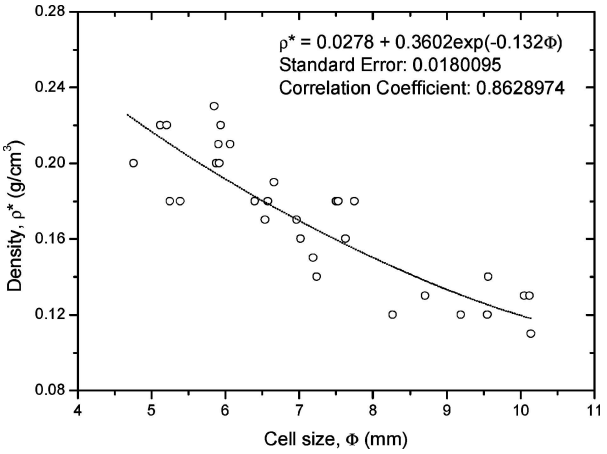

Figure 3 Relation of density and cell size of the aluminum foams.

spheroidal ones of Alporas foams of higher density [19]. The foam cells contain approximately 12–14 cell faces and 5 edges per face, the cell sizes of the closed cell foams span from 4 to 11 mm in diameter, and the densities of the foams vary from 0.1 to 0.22 g/cm^3.

Fig. 3 is the density plotted against cell size of the aluminum foams prepared at different processing conditions. The first order exponential decay was performed on the scattered data, and the obtained mathematical expression is given also in Fig. 3. Evidently, the density of the aluminum foams decreases with increasing cell size.

Fig. 4 shows the relationships of the cell wall thickness and node sizes versus cell size of the aluminum foams. Clearly, the node size, ϕ and the cell wall thickness of both $\delta_{1/2}$ and $\delta_{1/4}$ decrease with the increase in cell size, which is in good agreement with Simone and Gibson [18] where the data only for mid-span of the cell wall is given. Accordingly, the cell wall thickness, $\delta_{1/2}$ and $\delta_{1/4}$, are measured approximately 60–80 and 110–150 μm respectively, and the node size, ϕ approaches 160–205 μm for the foams with varied densities. The curves in Fig. 4 are the results of data fitting for the dimensions of the node size, ϕ, and cell wall thickness $\delta_{1/2}$ and $\delta_{1/4}$ at one-half and one-fourth of the chord length respectively. The node

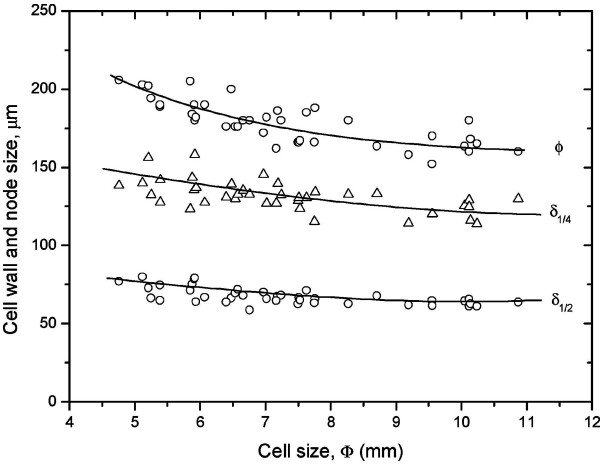

Figure 4 Relation of cell wall thickness and node size versus cell size of the aluminum foams.

size and the cell wall thickness of both $\delta/2$ and $\delta/4$ versus cell size obey the first order exponential decay and are expressed by $\phi = 159.64226 + 348.55\ e^{-0.42589\Phi}$ (standard error: 8.3640053 and correlation coefficient: 0.8120369), $\delta_{1/2} = 62.09 + 106.6{\cdot}e^{-0.443\Phi}$ (standard error of 3.3311301 and correlation coefficient of 0.7807902) and $\delta_{1/4} = 36.983 + 125.25{\cdot}e^{-0.03758\Phi}$ (standard error: 7.2896807 and correlation coefficient: 0.7162227).

Based on the dimension measurements of Φ, ϕ, $\delta_{1/2}$ and $\delta_{1/4}$ and the assumption of a pentagonal dodecahedron for the foam cells, the total surface area per cell is considered as $\pi\Phi^2$, and the area coverage per pentagon of the dodecahedron cell is determined as $\pi\Phi^2/12$. Then the edge length and centroid of the pentagon are determined, and the chord length, L is calculated by a straight line through the centroid between one angulus and its opposite edge of the pentagon face of the aluminum cells. As the cell geometry of the foams governs properties such as stiffness, yield strength, crush behavior and fracture resistance, therefore, the measurement and calculation of the foam cell parameters would provide the basis for the establishment of a computational model in more accordance with the cell structure for optimum performance of the closed cell aluminum foams.

3.2. Compression

In all of the compression tests, plastic collapse of the foam cells initiates in the top or/and bottom surface of the samples, and progresses inward in a pattern of successive collapse and densification. Fig. 5 shows the macrographs of the aluminum foam in different compression phases. At 5% strain, the collapse of the foam occurs at the bottom layer of the sample. With the increase in strain to 18%, the failure of the aluminum foam cells takes place at the top layer of the compression sample as well. As the compression continues, the deformation and collapse of the foam cells propagates layer by layer successively in the direction of the compression force into the middle of the compression specimen, sandwiching a visually perfect-shaped foam cell core between the densified top and bottom layers. For all the compression tests of the foams with different cell sizes, no initial failure is observed in the middle height of the foams. In fact, these walls may have experienced some plastic deformation prior to cell wall rupture. Furthermore, there is also no visible deformation of the mid-foam cells away from the collapsing interfaces, which also proves that the foams prepared in this study have relatively higher uniformities of cell structure and distribution.

The typical compressive stress-strain curves of the different density foams are shown in Fig. 6. After the first onset of initial foam cell failure, the plastic collapse stress drops. With increasing strain, the stress curve is serrated, and each serration corresponds to the fracture of the foam cell walls. Therefore, the curves in Fig. 6 represent typically a brittle foams. The plateau stress increases with increasing strain as the foam density increases, and the densification of the foams occurs at smaller strain with the increase in foam density.

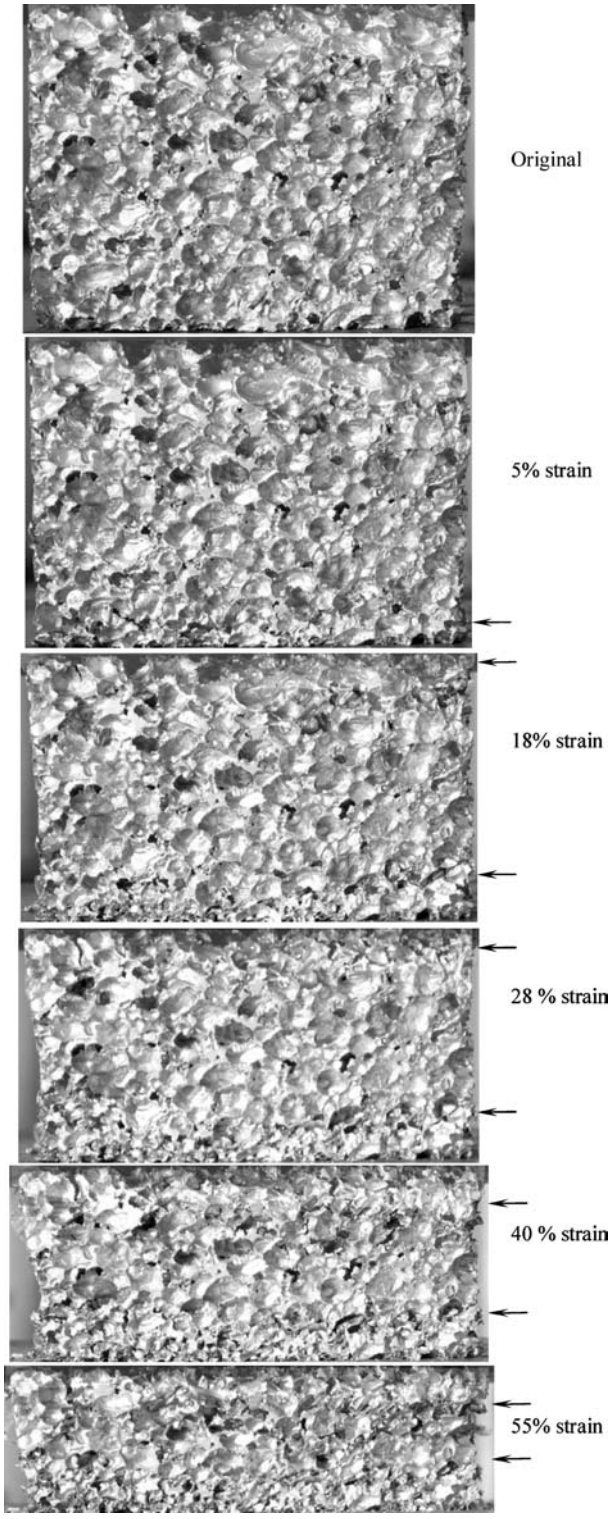

Figure 5 Macrographs of the aluminum foam compressed at different strain (the collapsing interfaces is indicated by arrows).

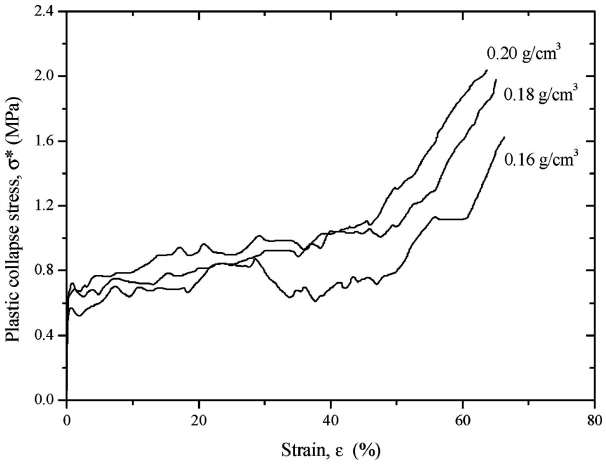

Figure 6 Compressive stress-strain curves of the foams with different densities.

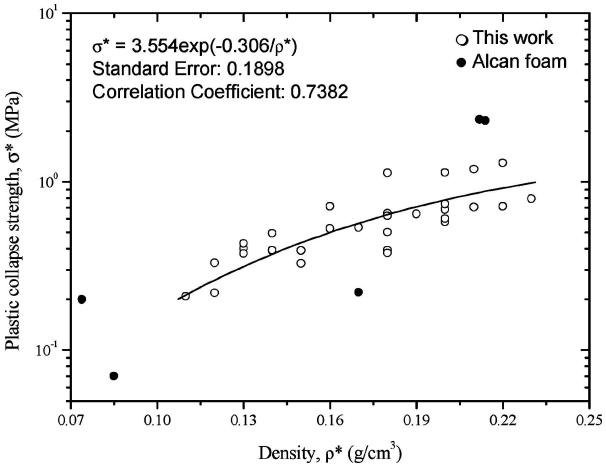

Figure 7 Relation of plastic collapse strength versus density of the aluminum foams.

The relationship between the plastic collapse strength and the density of the closed cell aluminum foams is illustrated in Fig. 7 in which a regression formula is given. With the increase in foam density, the plastic collapse strength of the foams is improved increasingly. The plastic collapse strength rises from 0.20 MPa for the 0.11 g/cm^3 foam to 1.29 MPa for the 0.22 g/cm^3 foam. That is more than five times increase in plastic collapse strength when the foam density is doubled, which means the significant impact of the foam density on plastic strength of the closed cell aluminum foam. Also included in Fig. 7 are the data of Alcan foams from Simone and Gibson [17]. The Alcan foam properties vary because the cell shape and orientation and the foam density vary throughout the thickness of the panel due to processing conditions. For example, an Alcan nominal 0.083 g/cm^3 foam had 0.188, 0.034 and 0.059 g/cm^3 approximately homogeneous sections from its bottom to top in 95 mm thickness, while the mean cell size of the Alcan foam was 7.93, 11.4 and 8.75 mm for the bottom, middle and top sections respectively [17]. Therefore, it is hard to compare the property of the two foams, although the two foams use essentially the same foaming technique. The Yong's modulus plotted against density of the closed cell foams is shown in Fig. 8 in which the data of Alcan foam are included [17]. The elastic modulus of the closed cell aluminum foams increases with the increasing foam density. However, the effect of density on elastic modulus of the foams is not so prominent as that on plastic collapse strength of the closed cell aluminum foams, for the elastic modulus of the closed cell aluminum foam increases from 0.70 to 1.17 GPa when the density changes from 0.11 to 0.22 g/cm^3.

The finite element simulations of a unit tetrakaidecahedral closed cell with flat faces give the normalized

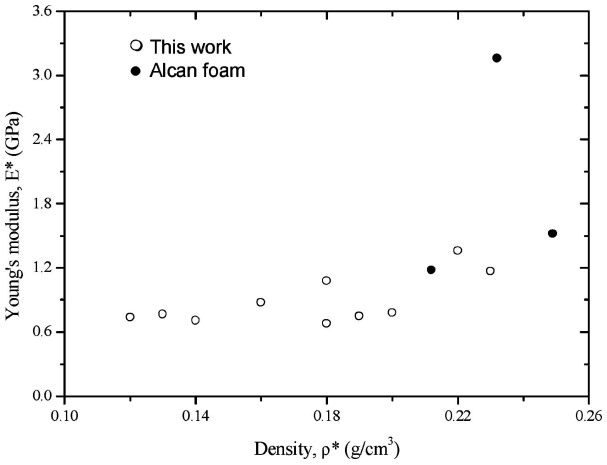

Figure 8 Relationship between Yong's modulus and density of the closed cell aluminum foams.

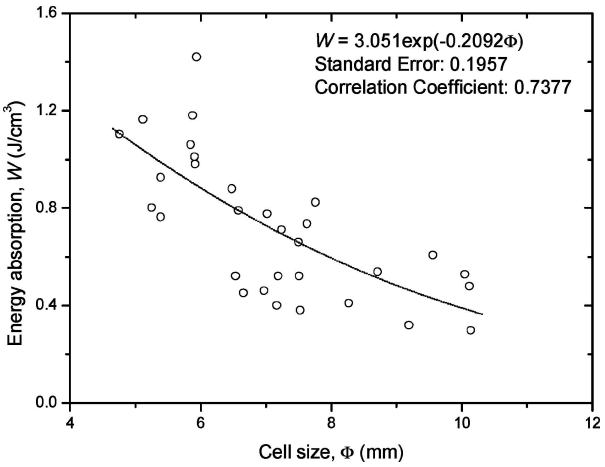

Figure 9 Energy absorption as a function of cell size of the aluminum foams.

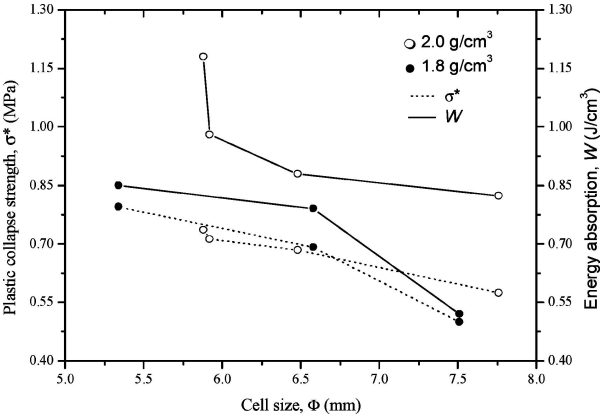

Figure 10 Relationship of plastic collapse strength and energy absorption versus cell size with different foam densities.

Yong's modulus as follows:

$$E^*/E_s = 0.32(\rho^*/\rho_s)^2 + 0.32(\rho^*/\rho_s)\,[8] \qquad (1)$$

For low density foams, the second linear density term dominates. Therefore, Equation 1 becomes

$$E^*/E_s = 0.32(\rho^*/\rho_s) \qquad (2)$$

Other similar simulations, on both tetrakaidecahedral closed cells and Weaire–Phelan closed cells give

$$E^*/E_s = 0.311(\rho^*/\rho_s)\,[19] \qquad (3)$$

Thus, Equations 2 and 3 are actually identical. For all of the foams, the density ρ_s and elastic modulus E_s of the cell wall solid are taken as 2.7 g/cm^3 and 70 GPa respectively. Through analysis, it is found that a perfect agreement of the experimental data with the equations is achieved if a constant, $C = 0.65$ is multiplies by the right side of the equations. That is, the fitting equation for the foams studied is

$$E^*/E_s = 0.208(\rho^*/\rho_s) \qquad (4)$$

The yield strength of the cell wall solid, σ_s is 300 MPa ($HV_{0.025} = 90$ kg/mm ^{2}) as measured from microhardness testing. Similarly, the normalized strength of the closed cell aluminum foams, σ^*/σ_s is established in direct relation to its relative density, ρ^*/ρ_s, and the formula is expressed by

$$\sigma^*/\sigma_s = c \cdot \rho^*/\rho_s \qquad (5)$$

where parameter c varies from 3.8 to 11.0 when the foam density changes from 0.11 to 0.22 g/cm^3.

The observed cell size dependence of the closed cell foams is depicted in the energy absorption versus cell size plot in Fig. 9 which also includes a fitting equation for the data. In contrast to the effect of foam density on plastic collapse strength, the energy absorption of the foams decreases rapidly with increasing cell size. For instance, the energy absorption of the aluminum foam drops from over unity to 0.3 J/cm^3 when cell size increases from 4.7 to 10.1 mm. Therefore, it is contradictory to meet the requirements of light weight, high strength and excellent energy absorption ability of the aluminum foams in engineering applications.

However, the performance of the closed cell aluminum foam changes with the control of its cell structure. As shown in Fig. 10, the improvements of plastic collapse strength and energy absorption ability of the closed cell aluminum foams are over 30% by the reduction of cell sizes for both 0.18 and 0.20 g/cm^3 foams, which is larger than expected in comparison with the work [11] where only less than 10% improvement is found by the effects of solid distribution on the modulus and strength of a foam. Based on the fact that the small-sized foam cells have relatively thicker cell wall and larger node size versus the large-sized ones with thinner walls and smaller nodes as shown in Fig. 4, it can be reasonably postulated that the better plastic collapse strength and energy absorption ability for the small-sized cells of the aluminum foams is attributed to their stronger cell structure which can withstand greater force before deformation and rapture. Furthermore, the thinner walls of larger sized cells of the same density corrugates and cracks more easily even at a very low stress level under compression load due to stress concentrations. Because the closed cells of the aluminum foams under compression load experience bending of the cell edges and stretching of

the cell faces [8], and the buckling of the cell walls is the dominant micromechanism of deformation in the closed cell foams [19], therefore, the control of cell wall thickness is critical as the compressive strength is governed purely by plastic yielding within the cell walls [18].

4. Conclusions

The density, node size and the cell wall thickness of the aluminum foams decrease with increasing cell size.

The failure of the foam cells under compressive load progresses successively from the top or/and bottom to the mid-layer of the compression specimens, and no initial rupture of the foam cells is observed in the mid-height of the foam samples.

When foam density increases from 0.11 to 0.22 g/cm^3, the plastic collapse strength rises from 0.20 to 1.29 MPa, while the elastic modulus of the closed cell aluminum foam increases from 0.70 to 1.17 GPa. In contrast, the energy absorption of the foams decreases rapidly with increasing cell size. When cell size increases from 4.7 to 10.1 mm, the energy absorption drops from over unity to 0.3 J/cm^3. The normalized Yong's modulus of the closed cell aluminum foam is $E^*/E_s = 0.208(\rho^*/\rho_s)$, while the normalized strength of the foams, σ^*/σ_s is expressed by $\sigma^*/\sigma_s = c\cdot\rho^*/\rho_s$ where c is a density-dependent parameter.

Furthermore, the plastic collapse strength and energy absorption ability of the closed cell aluminum foams are significantly improved by reducing cell size of the aluminum foams having the same density.

Acknowledgements

The authors gracefully acknowledge the financial supports of Nature Science Foundation of China, Contract NSFC 50371013 and Education Department of Liaoning Province,Contract No. 202033221.

References

1. T. MIYOSHI, M. ITOH, S. AKIYAMA and A. KITAHARA, *Adv. Engng. Mater.* **2** (4) (2000) 179.
2. W. J. CANTWELL, P. COMPSTON and G. REYES, *J. Mater. Sci. Lett.* **19**(24) (2000) 2205.
3. WEIGANG, CHEN, TOMASZ and WIERZBICKI, *Thin-Walled Struct.* **39**(4) (2001) 287.
4. A. -F. BASTAWROS, H. BART-SMITH and A. G. EVANS, *J. Mech. Phys. Solids.* **48**(2) (2000) 301.
5. L. D. KENNY, *Mater. Sci. Forum.* **217–222**(3) (1996) 1883.
6. IIJOON JIN, LORNE D. KENNY and HARRY SANG, Method of Producing Light Weight Foamed Metal, US Patent 4973358, 1990.
7. P. H. THORNTON and C. K. H. DHARAN, *Mater. Sci. Eng.* **18**(1) (1975) 97.
8. A. E. SIMONE and L. J. GIBSON, *Acta Mater.* **46** (1998) 2139.
9. WANG DEQING and SHI ZIYUAN, *Mater. Sci. Engng.* **A 361** (1–2) (2003) 45.
10. KATHRYN A. DANNEMANN and JAMES LANKFORD JR, *ibid.* **A293** (1–2) (2000) 157.
11. E. ANDREWS, W. SANDERS and L. J. GIBSON, *ibid.* **A270**(2) (1999) 113.
12. S. SANTOSA and T. WIERZBICKI, *J. Mech. Phys. Solids* **46**(4) (1998) 645.
13. I. W. HALL, M. GUDEN and C.-J. YU, *Scripta Materialia* **43**(6) (2000) 515.
14. A. PAUL and U. RAMAMURTY, *Mater. Sci. Engng.* **A281**(1–2) (2000) 1.
15. T. MUKAI, H. KANAHASHI, T. MIYOSHI, M. MABUCHI, T. G. NIEH and K. HIGASHI, *Scripta Materialia* **40**(8) (1999) 921.
16. A.-F. BASTAWROS, H. BART-SMITH and A. G. EVANS, *J. Mech. Phys. Solids* **48**(2) (2000) 301.
17. A. E. SIMONE and L. J. GIBSON, *Acta Materialia* **46**(9) (1998) 3109.
18. KATHRYN A. DANNEMANN and JAMES LANKFORD JR., *Mater. Sci. Engng.* **A293** (2000) 157.
19. A. M. KRAYNIK, M. K. NEILSEN, D. A. REINELT and W. E. WARREN, Foam Micromechanics, Foams and Emulsions, in Proceedings of the NATO Advanced Study Institute on 'Foams, Emulsions and Cellular Materials, Cargese, Corsica, 12–24 May, 1997, edited by J. F. Sadoc and N. Rivier (Kluwer Academic Publishers, Dordrecht, 1999) p. 259.

Received 8 September 2004
and accepted 12 January 2005